



# Nano-engineered PtVFe catalysts in proton exchange membrane fuel cells: Electrocatalytic performance

Bin Fang, Jin Luo, Peter N. Njoki, Rameshwori Loukrakpam, Bridgid Wanjala, Jian Hong, Jun Yin, Xiang Hu, Jordan Last, Chuan-Jian Zhong\*

Department of Chemistry, State University of New York at Binghamton, Binghamton, NY 13902, United States

## ARTICLE INFO

### Article history:

Received 31 October 2009

Received in revised form 10 February 2010

Accepted 13 February 2010

Available online 20 February 2010

### Keywords:

Nano-engineered trimetallic nanoparticles

Platinum–vanadium–iron nanoparticles

Electrocatalysts

Oxygen reduction reaction

PEM fuel cells

## ABSTRACT

Proton exchange membrane fuel cells (PEMFCs) are attractive because of their high conversion efficiency, low pollution, lightweight, and high power density. A major area of challenges is the design and engineering of active, robust, and low-cost electrocatalysts. This report discusses recent findings of our investigations of the design and nano-engineering of platinum–vanadium–iron catalysts for use in PEMFC. The membrane electrode assembly was prepared using nano-engineered PtVFe nanoparticles with controlled composition and size supported on carbon as cathode electrocatalysts. The electrocatalytic activity and stability of the catalysts have been characterized by both rotating disk electrode and membrane electrode assembly measurements. The trimetallic catalysts have been shown to exhibit excellent electrocatalytic performance in PEMFC in comparison with commercial platinum catalysts. The results exhibited a good agreement between obtained these two types of measurements in terms of the dependence on particle size, composition, and thermal treatment condition. The catalysts also showed good stability, which are potentially useful for practical application in PEMFCs.

© 2010 Elsevier Ltd. All rights reserved.

## 1. Introduction

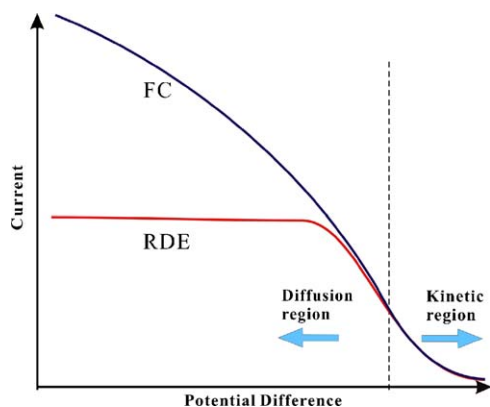
Fuel cells such as proton exchange membrane fuel cell (PEMFC) are attractive because of high conversion efficiency, low pollution, lightweight, and high power density. The potential applications range from power sources in automobiles and space shuttles to power grids for buildings and factories. However, one of the major challenges for the commercialization of fuel cell driven vehicles is the high overall manufacturing cost of PEMFCs. The cost of catalysts counts to 30% of the overall manufacturing cost because currently platinum catalysts are required for both anodes and cathodes in PEMFCs [1,2]. The lowering of Pt-loading in the catalysts, the improvement of the utilization of noble metals, and the increase of the stability of catalysts are some of the current approaches to reducing the high cost of catalysts for the ultimate commercialization of PEMFCs. The poor activity and poor durability of many existing Pt-based catalysts for the oxygen reduction reaction (ORR) in PEMFC's cathode are increasingly challenging problems as the evaluation of the pathways for platinum-loading reduction in the membrane electrode assemblies (MEAs) while increasing the activity becomes a focus of fuel cell research [1]. Because the lowering of the cathode loadings to about  $0.4 \text{ mg}_{\text{Pt}} \text{ cm}^{-2}$  is often limited by

the poor activity of Pt for ORR, two important pathways of research interests in the past decade include optimization of electrode structures and implementation of more active Pt-alloy catalysts [1]. The development of Pt-based multimetallic or alloy electrocatalysts is currently one promising area of finding effective solutions to the problem [2]. The preparation of most existing multimetallic or alloy catalysts were based on traditional catalyst-preparation methods such as co-precipitation and impregnation, which are often not adequate for controlling size and composition of the catalysts. In contrast, trimetallic nanoparticles such as PtVFe nanoparticles prepared by our nano-engineered synthesis and processing [3,4] have been shown to be an effective pathway for achieving controllable size and alloy composition ( $\text{Pt}_m\text{V}_n\text{Fe}_{100-m-n}$ ) that function as highly active electrocatalysts. The high electrocatalytic activity of the catalysts for ORR [3,4] is a result of the introduction of a second and third vanadium and iron atoms with smaller atomic sizes than platinum into the Pt-alloy which produces a combination of effects such as reduction of the lattice distance, the addition of surface sites for the formation of metal–oxygen bond and adsorption of hydroxide groups, and the modification of the d-band center.

While there have been numerous studies of bimetallic or trimetallic catalysts for increasing the electrocatalytic ORR activities using rotating disk electrode method [3–18], the evaluation of the fuel cell performance of the multimetallic or alloy catalysts has been rather limited [5,19–22]. The evaluation of the electrocatalytic activity and stability of ORR catalysts for PEM fuel cells

\* Corresponding author.

E-mail address: [cjzhong@binghamton.edu](mailto:cjzhong@binghamton.edu) (C.-J. Zhong).



**Scheme 1.** A schematic illustration of the different regions of the  $I$ - $V$  curves for fuel cell (FC) reactions obtained from measurements of rotating disk electrode (RDE) in an electrochemical cell and membrane electrode assembly (MEA) in a fuel cell.

has often been based on rotating disk electrode (RDE) characterization [3–18]. Relatively limited work has been performed with testing MEA in a fuel cell [5,19–25]. In fact, both RDE and MEA characteristics are comparable in the kinetic region (Scheme 1), but each provides important information on the catalyst performance from different perspectives in terms of catalyst activity, stability and measurement speed as well. In the kinetic region, the  $I$ - $V$  curves largely overlaps between RDE and MEA data because the ORR reactivity is largely determined by the catalyst's activity. Beyond this region, factors such as diffusion and cell resistance are also playing important roles in the overall reactivity. Fuel cell voltage is in general the summation of the thermodynamic potential  $E_{\text{Nernst}}$ , the total overvoltage associated with the electrochemical processes  $\eta_{\text{electrochemical process}}$  (from both anode and cathode overvoltages, i.e.,  $\eta_{\text{cathode}} - \eta_{\text{anode}}$ ), and the ohmic overvoltage  $\eta_{\text{ohmic}}$ , which can be expressed as [2]

$$E_{\text{cell}} = E_{\text{Nernst}} + \eta_{\text{electrochemical process}} - \eta_{\text{ohmic}}$$

where  $\eta_{\text{electrochemical process}} = \eta_{\text{catalyst}} - \eta_{\text{conc}}$ . The thermodynamic potential is governed by Nernst equation in terms of the standard cell voltage  $\Delta E_0$  (1.23 V) and the operating concentrations ( $P(\text{H}_2)$  and  $P(\text{O}_2)$ ). The total overvoltage associated with the electrochemical processes ( $\eta_{\text{electrochemical process}}$ ) is dependent on the overvoltages associated with the catalyst activity ( $\eta_{\text{catalyst}}$ ) and the concentration polarization ( $\eta_{\text{conc}}$ ). The activation overvoltage  $\eta_{\text{catalyst}}$  is mainly due to the sluggish activity of ORR, whereas  $\eta_{\text{conc}}$  reflects a combination of reactant and product fluxes through the MEA. The ohmic overvoltage ( $\eta_{\text{ohmic}}$ ) is due to a combination of resistances from the electron flow, proton flow, electrical contact, and membrane, the latter of which is proportional to the membrane thickness and inversely proportional to the membrane conductivity. RDE measurement has been the most frequently used method for evaluating ORR performance of catalysts because of its reduced speed in data acquisition in comparison with the time-consuming ORR performance evaluation in PEM fuel cells. However, the complication in data extraction from RDE curves has also led to some difficulties in comparing data from different sources [26]. In comparison with RDE characteristics beyond the kinetic region, the information from MEA fuel cell evaluation contains information from a combination of catalyst properties and cell optimization which are important for the ultimate application of catalysts in fuel cells.

Indeed our recent RDE and MEA measurements have demonstrated that the electrocatalytic activity of the nanostructured trimetallic PtVFe catalysts exhibited better performance than Pt catalysts [23]. While the detailed electrocatalytic activity and stability of bimetallic or trimetallic catalysts are affected by a com-

bination of electronic and geometric parameters such as Pt–Pt distance, d-band vacancy, particle size, and surface structure, these effects are often complex because of their dependences on catalyst-preparation and treatment methods. In this report, we describe the results of an investigation of several samples of PtVFe/C catalysts in terms of activity and stability based on both RDE and MEA performance measurements.

## 2. Experimental

### 2.1. Chemicals and synthesis

Platinum(II) acetylacetonate ( $\text{Pt}(\text{acac})_2$ , 97%), iron pentacarbonyl ( $\text{Fe}(\text{CO})_5$ ), 1,2-hexadecanediol ( $\text{CH}_3-(\text{CH}_2)_{13}-\text{CH}(\text{OH})-\text{CH}_2-\text{OH}$ , 90%), octyl ether ( $[\text{CH}_3(\text{CH}_2)_7]_2\text{O}$ , 99%), oleylamine ( $\text{CH}_3(\text{CH}_2)_7\text{CH}=\text{CH}(\text{CH}_2)_8\text{NH}_2$ , 70%), and oleic acid ( $\text{CH}_3(\text{CH}_2)_7\text{CH}=\text{CH}(\text{CH}_2)_7\text{COOH}$ , 99+%) were purchased from Aldrich and used as received. Vanadyl acetylacetonate ( $\text{VO}(\text{acac})_2$ , 97%) was purchased from Alfa Aesar, and were used as received. Other chemicals such as ethanol and hexane were purchased from Fisher Scientific.

The general reaction for the synthesis involves thermal decomposition and reduction reactions. The relative feed ratios of the metal precursors ( $\text{Pt}(\text{acac})_2$ ,  $\text{VO}(\text{acac})_2$ , and  $\text{Fe}(\text{CO})_5$ ) were controlled for achieving the desired ternary composition in the nanoparticles produced. The nanoparticle product is soluble in the reaction solution, and can be collected by precipitation method. Details of the synthesis are described in previous reports [3,4].

Typically, 140 mg carbon black (Vulcan XC-72R) and 66 mg of the as-synthesized PtVFe nanoparticles (e.g.,  $\text{Pt}_{35}\text{V}_{23}\text{Fe}_{42}$ , and  $\text{Pt}_{42}\text{V}_{19}\text{Fe}_{39}$ , and  $\text{Pt}_{59}\text{V}_{11}\text{Fe}_{30}/\text{C}$ ) were used to produce the carbon-supported PtVFe catalysts, which were calcined by thermal treatment at 300–450 °C under oxygen and hydrogen atmosphere respectively. Details of the synthesis, preparation and thermal treatment are described in previous reports [3,4].

Glassy carbon (GC) disks (geometric area: 0.196 cm<sup>2</sup>) were polished with 0.03  $\mu\text{m}$   $\text{Al}_2\text{O}_3$  powders, followed by careful rinsing with deionized water. The geometric area of the GC electrode provides a measure of the loading of catalyst on the electrode surface used for the voltammetric characterization.

Nafion™ 212 membrane, Teflon™ treated Toray™ carbon paper were purchased from Electrochem Inc. 20% Pt/C catalyst was purchased from E-tek.

### 2.2. Instrumentation and measurements

The following techniques were used for the characterization of the nanoparticles and catalysts.

#### 2.2.1. Transmission electron microscopy

Transmission electron microscopy (TEM) was performed on Hitachi H-7000 electron microscope (100 kV). For TEM measurements, the catalyst samples were suspended in hexane solution and were drop cast onto a carbon-coated copper grid followed by solvent evaporation in air at room temperature.

#### 2.2.2. Direct current plasma–atomic emission spectroscopy

The composition was analyzed using the direct current plasma–atomic emission spectroscopy, which was performed using an ARL Fisons SS-7 direct current plasma–atomic emission spectrometer (DCP–AES). Measurements were made on emission peaks at 265.95, 309.311 and 259.94 nm for Pt, V and Fe, respectively. The nanoparticle samples were dissolved in concentrated aqua regia, and then diluted to concentrations in the range of 1–50 ppm for analysis. Calibration curves were made from dissolved standards with concentrations from 0 to 50 ppm in the same

acid matrix as the unknowns. Detection limits, based on three standard deviations of the background intensity, are 0.02, 0.002 and 0.005 ppm for Pt, V and Fe. Standards and unknowns were analyzed 10 times each for 3 s counts. Instrument reproducibility, for concentrations greater than 100 times the detection limit, results in  $\pm 2\%$  error. The metal composition was expressed as  $\text{Pt}_{n1}\text{V}_{n2}\text{Fe}_{n3}$ , where  $n1$ ,  $n2$  and  $n3$  represent the atomic percentage of the element in the ternary catalyst.

### 2.2.3. Thermogravimetric analysis

Thermogravimetric analysis (TGA) was performed on a Perkin-Elmer Pyris 1-TGA for determining the metal loading on carbon black. Typical samples weighed  $\sim 4$  mg and were heated in a platinum pan. Samples were heated in 20%  $\text{O}_2$  at a rate of  $10^\circ\text{C min}^{-1}$ .

### 2.2.4. Electrochemical characterization

The electrode was coated with the catalyst layer using modified method from previous reports [3,4]. Briefly, a typical suspension of the catalysts was prepared by suspending 1.0 mg catalysts (PtVFe/C) in 1 mL Millipore water with diluted (5% vol.) Nafion™ (5wt%, Aldrich). The suspension was then quantitatively transferred to the surface of the polished GC disk. The electrodes were dried overnight at room temperature. The electrochemical activity for oxygen reduction was measured using the hydrodynamic rotating disk electrode technique. The standard three-electrode configuration was used for the cell, and the reference and counter electrodes were in separate compartments of the electrochemical cell. Glassy carbon-based working electrode with a geometric surface area of  $0.196\text{ cm}^2$  was used, and  $10\ \mu\text{l}$  catalyst ink was pipetted and uniformly distributed over the glassy carbon surface. To prepare catalyst ink, 20 mg supported catalysts were mixed with 20 ml Milli-Q water and 1 ml diluted Nafion solution (5 wt%, Aldrich). The solution was ultrasonicated using a pulse ultrasonic probe for 10 min or until a dark, uniform ink was achieved. Cyclic voltammetry (CV) was performed at room temperature to clean the catalysts surface. Optimal grade sulfuric acid (Fisher Scientific) diluted with Milli-Q water to 0.5 M was used as electrolyte, and it was deaerated with high purity nitrogen before the measurement. The potentials were controlled with respect to the reference hydrogen electrode by a potentiostat from CH Instruments and reported with respect to reversible hydrogen electrode (RHE). The RDE measurements were performed using a rotating disk electrode system made by Pine Instrument. Before the measurement, the sulfuric acid was saturated with pure oxygen. All measurements were performed under the rotating speed of 1600 rpm.

### 2.2.5. Fuel cell performance evaluation

MEAs ( $5\text{ cm}^2$  active area) used in this study were prepared by conventional catalyst-coated substrate (CCS) method. The electrocatalyst–Nafion ink was painted on a wet-proofed carbon paper (Toray™ EC-TP1-060T). The MEAs were prepared using  $\text{Pt}_{42}\text{V}_{19}\text{Fe}_{39}/\text{C}$  catalyst (21% and 22% metal loading,  $0.4\text{ mg}_{\text{Pt}}\text{ cm}^{-2}$ ) for the cathode and Pt/C catalyst (20% Pt/C, E-tek,  $0.4\text{ mg}_{\text{Pt}}\text{ cm}^{-2}$ ) for the anode. For  $\text{Pt}_{35}\text{V}_{23}\text{Fe}_{42}/\text{C}$  catalyst, a loading of  $0.7\text{ mg}_{\text{Pt}}\text{ cm}^{-2}$  ( $1.0\text{ mg cm}^{-2}$  metal loading) was used to prepare the cathode electrode (The anode was Pt/C with a loading of  $1.0\text{ mg}_{\text{Pt}}\text{ cm}^{-2}$ ). The PEMFC performance of this PtVFe sample was compared with the performance data for Pt/C catalyst (20% Pt/C, E-tek,  $1.0\text{ mg}_{\text{Pt}}\text{ cm}^{-2}$ ). To enhance its adhesion to the Nafion 212 membrane, a thin coating of 5 wt% Nafion solution was brushed onto the active side of the electrodes to produce a Nafion loading of  $\sim 0.4\text{ mg cm}^{-2}$ . For comparison, MEAs were also prepared using Pt/C (20% Pt/C, E-tek,  $0.4\text{ mg}_{\text{Pt}}\text{ cm}^{-2}$ ) catalyst for both anode and cathode. The MEAs were prepared by hot pressing the sandwich structured Nafion™ 212 membrane (DuPont) and catalyst-coated electrodes at  $120^\circ\text{C}$ . The hot pressed MEAs were placed in a standard fuel cell test cell

using gold-coated copper plates as current collector. The fuel cell was tested in a single-cell test station (Electrochem Inc.). The testing conditions included 100% humidified  $\text{H}_2$  for the anode and 100% humidified  $\text{O}_2$  for the cathode, each with a flow rate of  $100\text{ mL min}^{-1}$ , a back pressure of 30 psi, and an operating temperature of  $75^\circ\text{C}$ . The MEA was conditioned in the fuel cell for 1 h before recording the polarization curves.

## 3. Results and discussion

The as-synthesized PtVFe nanoparticles were shown in our previous reports [3,4] to exhibit controllable size (2–4 nm), composition ( $\text{Pt}_m\text{V}_n\text{Fe}_{100-m-n}$ ) with uniform trimetallic alloy distribution regardless of size [4,10,12]. In this report, we focused on investigating the trimetallic nanoparticle catalysts with controlled composition such as  $\text{Pt}_{35}\text{V}_{23}\text{Fe}_{42}/\text{C}$  and  $\text{Pt}_{42}\text{V}_{19}\text{Fe}_{39}/\text{C}$ . The average particle size for the carbon-supported nanoparticle catalysts after calcination treatment was 3–4 nm. The electrochemical and electrocatalytic characteristics for the nano-engineered PtVFe/C catalysts were compared with Pt/C catalyst (E-tek, 2–3 nm) based on cyclic voltammetry, RDE, and MEA evaluation in fuel cells.

Fig. 1 shows a representative set of TEM micrographs and size distributions for three PtVFe/C catalysts (Catalysts A–C) prepared under slightly different conditions. Catalyst A, i.e.,  $\text{Pt}_{35}\text{V}_{23}\text{Fe}_{42}/\text{C}$ , was prepared with a lower percentage of Pt in the trimetallic composition. In comparison, Catalysts B and C were prepared with a higher Pt percentage in the trimetallic nanoparticles, i.e.,  $\text{Pt}_{42}\text{V}_{19}\text{Fe}_{39}/\text{C}$ . The difference of the preparation between these two catalysts was the dispersion of the nanoparticles on the carbon support. Catalyst C had a better dispersion than Catalyst B because of a difference in concentration of the nanoparticles and carbon support used in the dispersion. A lower concentration was used for the preparation of Catalyst C which led to a better dispersion than the case of Catalyst B.

As shown in Fig. 1, the average particle size of Catalyst A was  $3.5 \pm 0.7\text{ nm}$  for Catalyst A. An increased percentage of Pt in the trimetallic composition, e.g., Catalysts B and C, was found to exhibit to an increased particle size, e.g.,  $4.8 \pm 1.7\text{ nm}$  for B and  $4.3 \pm 0.5\text{ nm}$  for C. Apparently, the Catalyst B exhibited somewhat larger size and poorer monodispersity than those for Catalyst C. The size and composition of these carbon-supported nanoparticle catalysts can be correlated with their phase properties, which is part of our on-going investigation using x-ray diffraction technique for the characterization.

### 3.1. Determination of electrochemical active area

The hydrogen adsorption/desorption characteristics were obtained with glassy carbon electrode inked with the catalyst using CV technique, which provided a measure of the electrochemical active area (ECA) of the catalysts. The potential was cycled between 0.02 and 1.15 V (vs. RHE) at  $20\text{ mV s}^{-1}$  in a solution of 0.5 M  $\text{H}_2\text{SO}_4$  purged with nitrogen at  $25^\circ\text{C}$ . Fig. 2 shows a representative set of CV data, which are characteristic of the surface hydrogen and oxide adsorption/desorption for Pt/C and PtVFe/C catalysts. The CV curves exhibit well-defined hydrogen adsorption/desorption peaks in the potential region of 0–0.4 V and adsorption/desorption peaks for surface oxide species at 0.7 and 1.0 V [13]. In comparison with the peaks observed for Pt/C, the peaks observed for PtVFe/C catalysts are similar but less resolved in the hydrogen adsorption/desorption potential region.

From the current under the hydrogen adsorption peaks, ECA values were determined, yielding  $66\text{ m}^2\text{ g}^{-1}_{\text{Pt}}$  for Pt/C and  $85\text{ m}^2\text{ g}^{-1}_{\text{Pt}}$  for Catalyst A ( $\text{Pt}_{35}\text{V}_{23}\text{Fe}_{42}/\text{C}$ ). Note that the ECA varies that we obtained with the commercial catalysts were found to vary

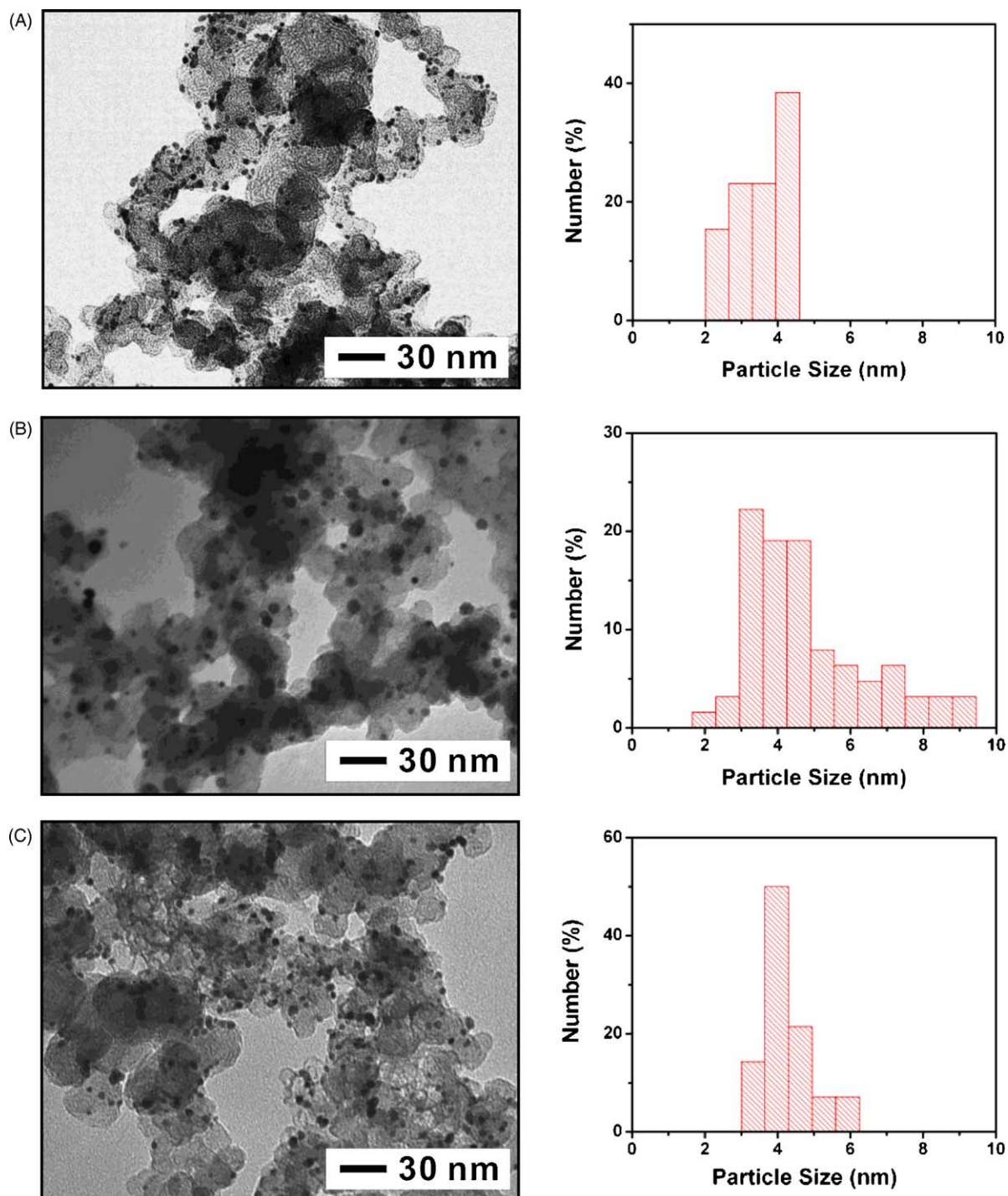


**Fig. 1.** TEM micrographs and size distributions for three catalysts: (A)  $\text{Pt}_{35}\text{V}_{23}\text{Fe}_{42}/\text{C}$  ( $3.5 \pm 0.7$  nm) (Catalyst A), (B)  $\text{Pt}_{42}\text{V}_{19}\text{Fe}_{39}/\text{C}$  ( $4.8 \pm 1.7$  nm) (Catalyst B), and (C)  $\text{Pt}_{42}\text{V}_{19}\text{Fe}_{39}/\text{C}$  ( $4.3 \pm 0.5$  nm) (Catalyst C).

from 60 to 90 from sample to sample, which was possibly due to inhomogeneity of the catalysts. The difference between Pt/C and  $\text{Pt}_{35}\text{V}_{23}\text{Fe}_{42}/\text{C}$  catalysts is consistent with the analysis of the double-layer capacitive behavior in the potential window between the hydrogen and oxide reaction regions (0.4–0.6 V). The capacitive currents correspond to charging or discharging of the electric double-layer at the interface between the catalyst-coated electrode and the electrolyte. The double-layer capacitance value was found to be  $116 \text{ F g}^{-1}_{\text{PtVFe/C}}$  (or  $148 \text{ F g}^{-1}_{\text{C}}$ ) for Catalyst A, which was much larger than that of Pt/C ( $48 \text{ F g}^{-1}_{\text{Pt/C}}$  (or  $60 \text{ F g}^{-1}_{\text{C}}$ )). The ECA value determined for Catalyst B ( $\text{Pt}_{42}\text{V}_{19}\text{Fe}_{39}/\text{C}$ ) was  $46 \text{ m}^2 \text{ g}^{-1}_{\text{Pt}}$ ,

smaller than that for Catalyst A. The double-layer capacitance value was found to be  $122 \text{ F g}^{-1}_{\text{PtVFe/C}}$  (or  $143 \text{ F g}^{-1}_{\text{C}}$ ). For Catalyst C ( $\text{Pt}_{42}\text{V}_{19}\text{Fe}_{39}/\text{C}$ ), the ECA value determined from the CV curve,  $54.6 \text{ m}^2 \text{ g}^{-1}_{\text{Pt}}$ , was also smaller than Catalyst A, but comparable with that for Catalyst B. In this case, the double-layer capacitance value was found to be  $92 \text{ F g}^{-1}_{\text{PtVFe/C}}$  (or  $116 \text{ F g}^{-1}_{\text{C}}$ ).

The results from the ECA data seemed to be quite consistent with the difference in particle sizes between the catalysts of the two different compositions ( $3.5 \pm 0.7$  nm for Catalyst A, and  $4.8 \pm 1.7$  nm for Catalyst B,  $4.3 \pm 0.5$  nm for Catalyst C). The difference between catalysts B and C was relatively small, which appeared to be con-

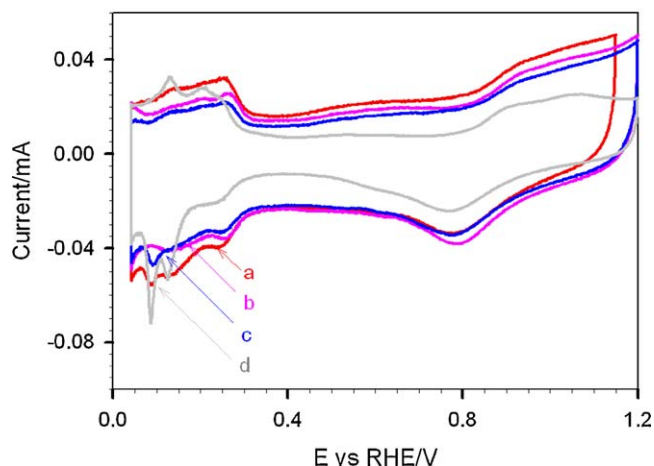


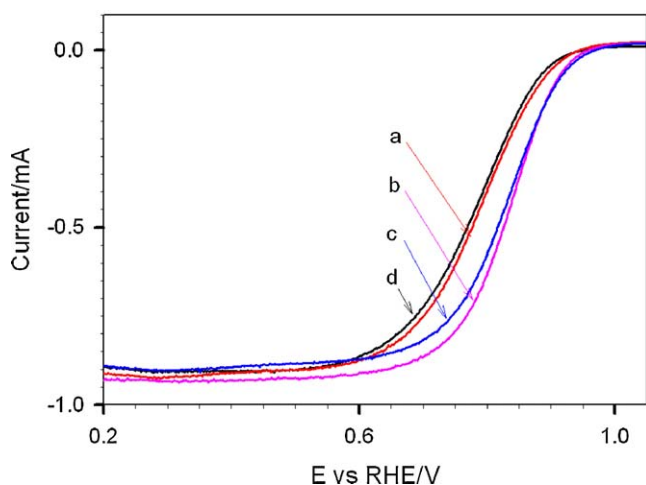
**Fig. 2.** Cyclic voltammograms for catalysts of PtVFe/C ( $\text{Pt}_{35}\text{V}_{23}\text{Fe}_{42}/\text{C}$  (a),  $\text{Pt}_{42}\text{V}_{19}\text{Fe}_{39}/\text{C}$  (b), and  $\text{Pt}_{42}\text{V}_{19}\text{Fe}_{39}/\text{C}$  (c)) and Pt/C (d) on a GC electrode ( $0.196\text{ cm}^2$ ) in  $0.5\text{ M H}_2\text{SO}_4$  electrolyte saturated with  $\text{N}_2$ . Scan rate:  $20\text{ mV s}^{-1}$ .

sistent with the small difference in the average particle sizes of the two catalysts.

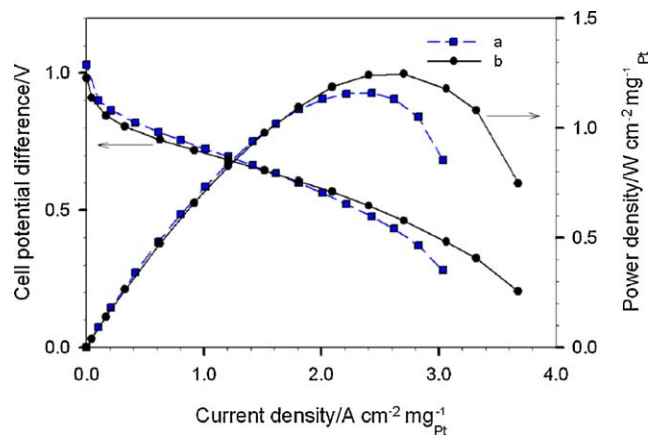
### 3.2. Characterization of electrocatalytic activity by RDE

Fig. 3 shows a representative set of RDE curves comparing the ORR activities for Pt/C and PtVFe/C catalysts in  $0.5\text{ M H}_2\text{SO}_4$  electrolyte. The kinetics currents at  $0.858\text{ V}$  (vs. RHE) were used to determine the Pt-mass activity and specific activity. For Catalyst A, the kinetics current measured at  $0.858\text{ V}$  showed  $2.13 \times 10^{-4}\text{ A}$ . In comparison with Pt/C catalyst ( $1.68 \times 10^{-4}\text{ A}$ ) under the same condition, the small increase of the current in the kinetic region is indicative of a higher electrocatalytic activity for the trimetallic catalyst than that for the Pt catalyst [3]. Indeed, the Pt-mass activity was found to be  $0.14\text{ A mg}^{-1}_{\text{Pt}}$  for PtVFe/C catalyst, which is 1.7 times larger than that for Pt/C ( $0.08\text{ A mg}^{-1}_{\text{Pt}}$ ).

For Catalyst B, the kinetics current at  $0.858\text{ V}$  showed  $3.16 \times 10^{-4}\text{ A}$ . The Pt-mass activity calculated from the RDE data at  $0.858\text{ V}$  was  $0.30\text{ A mg}^{-1}_{\text{Pt}}$ , which is 3.5 times larger than that for Pt/C ( $0.084\text{ A mg}^{-1}_{\text{Pt}}$ ). For Catalyst C, the kinetics current at  $0.858\text{ V}$  showed a value of  $2.95 \times 10^{-4}\text{ A}$ . This value translates to a Pt-mass activity of  $0.28\text{ A mg}^{-1}_{\text{Pt}}$ , which is 3.3 times greater than that for



**Fig. 3.** RDE for ORR using different catalysts:  $\text{Pt}_{35}\text{V}_{23}\text{Fe}_{42}/\text{C}$  (a),  $\text{Pt}_{42}\text{V}_{19}\text{Fe}_{39}/\text{C}$  (b), and  $\text{Pt}_{42}\text{V}_{19}\text{Fe}_{39}/\text{C}$  (c) and standard Pt/C (20%) (d) on glassy carbon electrode (loading  $10\text{ }\mu\text{g}$ ,  $0.196\text{ cm}^2$ ) in  $0.5\text{ M H}_2\text{SO}_4$ . Scan rate:  $10\text{ mV s}^{-1}$ , and rotating speed:  $1600\text{ rpm}$ .



**Fig. 4.** Polarization and power density curves of MEAs with  $\text{Pt}_{35}\text{V}_{23}\text{Fe}_{42}/\text{C}$  (a) and Pt/C (b) as cathode catalyst in PEMFC at  $75\text{ }^\circ\text{C}$ . Note that normalized current density was used in this plot because of the difference in catalyst loading between MEAs with Pt/C ( $1.0\text{ mg}_{\text{Pt}}\text{ cm}^{-2}$ ) and PtVFe/C ( $0.7\text{ mg}_{\text{Pt}}\text{ cm}^{-2}$ ).

Pt/C ( $0.084\text{ A mg}^{-1}_{\text{Pt}}$ ), indicating that there is a higher electrocatalytic activity for the trimetallic catalyst than that for the Pt catalyst [10]. The ECA, mass activity and specific activity data are summarized in Table 1. The mass activity was shown to increase with the increase of Pt percentage in the trimetallic catalysts when the percentages of the other two metals were comparable. Again, the difference in mass activity between Catalysts B and C was relatively small, implying an insignificant contribution of the small difference in the average particle sizes of the two catalysts.

### 3.3. Evaluation of electrocatalytic performance in PEM fuel cell

To ensure that the PEMFC testing conditions in our system were appropriate, polarization curves were first obtained using a commercial MEA (Electrochem. Inc.) with Pt/C catalysts ( $20\%\text{ Pt/C}$ ,  $1.0\text{ mg}_{\text{Pt}}\text{ cm}^{-2}$  at both anode and cathode) in a  $5\text{-cm}^2$  fuel cell under an operating temperature of  $75\text{ }^\circ\text{C}$ . In comparison with the data provided by the commercial source for the MEA [27], little difference was observed in the  $I$ - $V$  curves for the MEA under our testing condition. This result validates the measurement conditions of our system for the FC performance evaluation.

MEAs with the trimetallic catalysts were evaluated in the PEM fuel cell to determine its fuel cell performance. Fig. 4 shows a representative set of PEMFC performance data for  $\text{Pt}_{42}\text{V}_{19}\text{Fe}_{39}/\text{C}$  (Catalyst A) in comparison with the data for Pt/C catalysts at  $75\text{ }^\circ\text{C}$ . The MEA with Pt/C catalyst exhibited a value of  $0.72\text{ V}$  at  $1.0\text{ A cm}^{-2}$ . This value is largely comparable to those reported under similar operation conditions using CCS method for the MEA fabrication [28], thus validating the quality and effectiveness of our MEA preparation for the evaluation of the fuel cell performance in comparing PtVFe/C and Pt/C catalysts.

For Catalyst A, the FC performance data in terms of polarization curve and power density were compared with the Pt/C catalyst. Since different catalyst loadings were used for MEAs with Pt and PtVFe/C catalysts, the normalized current density was used for the comparison. At  $75\text{ }^\circ\text{C}$ , the peak power density of Pt/C was found at  $2.43\text{ A cm}^{-2}\text{ mg}_{\text{Pt}}$  and  $1.16\text{ W cm}^{-2}\text{ mg}_{\text{Pt}}$  at  $0.47\text{ V}$ , whereas that of PtVFe was at  $2.70\text{ A cm}^{-2}\text{ mg}_{\text{Pt}}$  and  $1.25\text{ W cm}^{-2}\text{ mg}_{\text{Pt}}$  at  $0.46\text{ V}$ . The power densities reached the maximum at a similar potential. PtVFe/C fuel cell had a  $\sim 10\%$  higher peak power density per mg Pt than that of Pt/C at both room and high temperatures. The PtVFe/C catalyst showed a better performance than Pt/C catalyst, which is consistent with the activity trend from the RDE data.

A close examination of the polarization curves in the lower current density region ( $<1.5\text{ A cm}^{-2}$  @  $75\text{ }^\circ\text{C}$ ) however indicates that

**Table 1**  
Comparison of ECA, RDE, and FC data for Pt/C and Catalysts A, B and C.

Catalyst	ECA ( $\text{m}^2 \text{g}^{-1} \text{Pt}$ )	Mass activity ( $\text{A mg}^{-1} \text{Pt}$ )	Specific activity ( $\text{mA cm}^{-2}$ )	$I(\text{FC}) @ 0.65 \text{ V}$ ( $\text{A cm}^{-2} \text{mg}^{-1} \text{Pt}$ )	Peak power density ( $\text{W cm}^{-2} \text{mg}^{-1} \text{Pt}$ )
Pt/C	66	0.084	0.13	1.5	1.16
Pt <sub>35</sub> V <sub>23</sub> Fe <sub>42</sub> /C (A)	85	0.14	0.16	1.5	1.24
Catalyst	ECA ( $\text{m}^2 \text{g}^{-1} \text{Pt}$ )	Mass activity ( $\text{A mg}^{-1} \text{Pt}$ )	Specific activity ( $\text{mA cm}^{-2}$ )	$I(\text{FC}) @ 0.65 \text{ V}$ ( $\text{A cm}^{-2}$ )	Peak power density ( $\text{W cm}^{-2}$ )
Pt/C	66	0.084	0.13	0.5	0.52
Pt <sub>42</sub> V <sub>19</sub> Fe <sub>39</sub> /C (B)	46	0.30	0.65	1.0	0.76
Pt <sub>42</sub> V <sub>19</sub> Fe <sub>39</sub> /C (C)	55	0.28	0.51	0.9	0.82

Note: Under the same RDE measurement conditions as for these catalysts, the values of ECA, mass activity, and specific activity for Pt/C were  $66 \text{ m}^2 \text{g}^{-1} \text{Pt}$ ,  $0.084 \text{ A mg}^{-1} \text{Pt}$ , and  $0.13 \text{ mA cm}^{-2}$ , respectively. The potential setting at  $0.858 \text{ V}$  allows data comparison with those reported for  $0.900 \text{ V}$  in  $0.1 \text{ M HClO}_4$ .

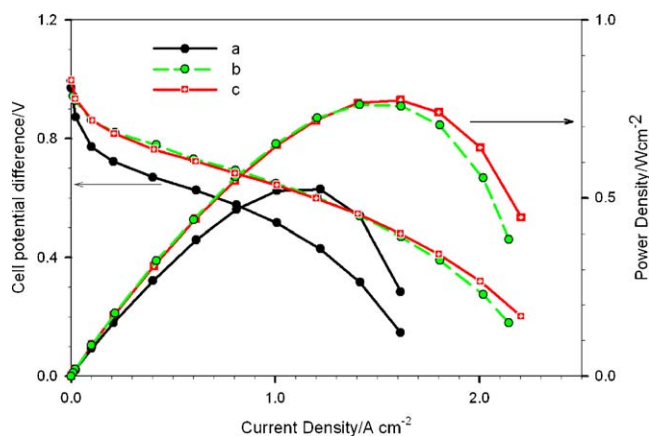
the  $I$ - $V$  curves for PVF fuel cell are somewhat lower than that of Pt/C fuel cell. One possible reason for this is the lack of full hydration of the PVF/C catalyst at low-current densities leading to a less active surface area. When the current density is increased, the catalyst layer was better hydrated due to an increased water production rate, which increased the active surface area and thus the catalytic activity [21]. Another reason could be due to resistance to the flow of ions in the electrolyte and resistance to flow of electrons through the electrode [22]. A comparison for electronic resistance of MEAs with Pt/C and PVF/C indicated a higher resistance for the MEA with the PtVFe/C catalyst.

Fig. 5 shows a representative set of fuel cell performance data comparing the data for Catalysts B and C with that for Pt/C catalyst. The comparison was under the condition of  $0.4 \text{ mg}_{\text{Pt}} \text{ cm}^{-2}$  for each catalyst. It is evident that both the cell voltage and the power density for the fuel cell with PtVFe/C catalyst in the cathode are higher than those for the cell with the Pt/C catalyst under  $75^\circ \text{C}$ . At  $75^\circ \text{C}$ , the peak power density of Pt/C was found to yield  $1.3 \text{ A cm}^{-2}$  and  $0.53 \text{ W cm}^{-2}$  at  $0.43 \text{ V}$ , whereas that for Catalyst B was at  $1.62 \text{ A cm}^{-2}$  and  $0.76 \text{ W cm}^{-2}$  at  $0.47 \text{ V}$ . The power densities reached the maximum at a similar potential. The PtVFe/C fuel cell exhibited a 40% higher peak power density than that of Pt/C at both room and high temperatures. This finding demonstrates that PtVFe/C catalyst has a better performance than Pt/C catalyst, which is consistent with the activity trend revealed by the RDE data. For Catalyst C, the peak power density was found to yield  $1.81 \text{ A cm}^{-2}$  and  $0.82 \text{ W cm}^{-2}$  at  $0.45 \text{ V}$ . The power densities for both Pt/ and Pt<sub>42</sub>V<sub>19</sub>Fe<sub>39</sub>/C catalysts reached the maximum at the similar

cell voltage ( $0.4$ – $0.5 \text{ V}$ ). The fuel cell with PtVFe/C cathode catalyst showed a 50% increase in peak power density in comparison with that with Pt/C catalyst.

Table 1 summarizes the ECA, RDE, and FC data for Pt/C and Catalysts A, B and C. These results demonstrate the excellent performance of the PtVFe/C catalyst in PEM fuel cell, which is better than Pt/C catalyst. The finding is also consistent with the electrocatalytic activity trend revealed by the RDE data.

While the fuel cell performance in the high-current density region is dependent on a combination of catalyst activity and other optimization parameters (e.g., ohmic and mass transport losses), the observation of at least twofold increase in current density for PtVFe/C at  $0.9 \text{ V}$  in the low-current density region (i.e., kinetic region) which is only dependent on the catalyst activity is clearly indicative of a better performance of the PtVFe/C than the Pt/C catalyst. By comparing the FC performance data in terms of polarization curve and power density between our PtVFe/C (B) catalyst and the commercial Pt/C (A) catalyst, the most important observation is that both the cell voltage and the power density for the fuel cell with PtVFe/C catalyst in the cathode are overall higher than those for the cell with the Pt/C catalyst under both temperatures. A quantitative comparison of the data with the literature data for fuel cell performance using other bimetallic or trimetallic catalysts was not attempted at this point because of the differences in MEA materials and preparations which could lead to different IR contribution to the fuel cell  $I$ - $V$  data, as supported by a preliminary examination of the IR-corrected  $I$ - $V$  curves using a resistance value of  $0.08 \Omega \text{ cm}^2$  for  $50\text{-}\mu\text{m}$  Nafion™ 212 membrane [28,29], suggesting that further optimization of the MEA preparation is needed.



**Fig. 5.** Polarization and power density curves of MEAs with Pt/C (a), and Pt<sub>42</sub>V<sub>19</sub>Fe<sub>39</sub>/C (b and c) as cathode catalysts in PEMFC at  $75^\circ \text{C}$ . b and c correspond to Catalysts B and C, respectively. Pt-loading in both anode and cathode was  $0.4 \text{ mg}_{\text{Pt}} \text{ cm}^{-2}$ .

### 3.4. Catalyst stability

A preliminary study of the stability of the PtVFe/C catalysts was also performed by both RDE and MEA FC measurements. The stability of the catalysts was examined by comparing the activities between fresh catalysts and catalysts after extensive electrochemical cyclings in the reaction potential window. In the measurement of a separate catalyst sample, the RDE data (Fig. 6) were compared in terms of electrocatalytic activity and stability of PtVFe/C catalysts before and after 5000 cycles between  $0.45$  and  $1.05 \text{ V}$  (vs. RHE,  $0.1 \text{ M HClO}_4$ ).

In this example, the catalyst before electrochemical cycling showed an ECA value of  $53.6 \text{ m}^2 \text{g}^{-1} \text{Pt}$ , Pt specific activity of  $0.59 \text{ mA cm}^{-2}$  and Pt-mass activity of  $0.32 \text{ A mg}^{-1} \text{Pt}$ . The catalyst after 5000 cycles showed a Pt-mass activity of  $0.37 \text{ A mg}^{-1} \text{Pt}$ . The catalyst after 5000 cycles showed about 20% increase in mass activity. Based on the RDE data obtained after 5000 potential cycles between  $0.45$  and  $1.05 \text{ V}$ , there was no indication of any noticeable decrease in the kinetic current.

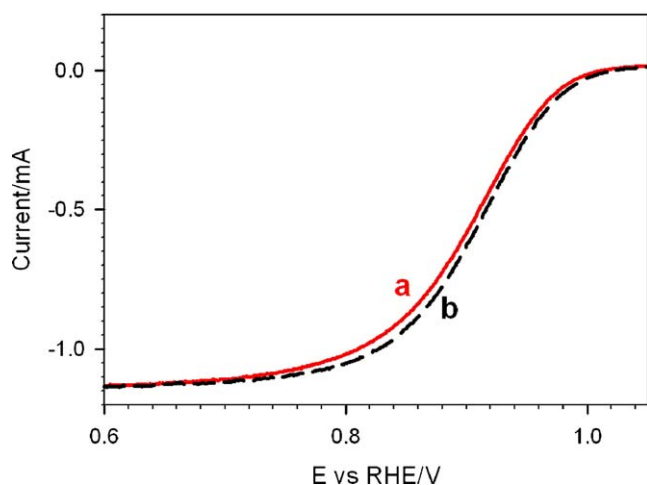


**Fig. 6.** RDE curves for ORR in 0.1 M  $\text{HClO}_4$  electrolyte saturated with  $\text{O}_2$  before (a) and after (b) 5000 cycles (scan rate:  $10 \text{ mV s}^{-1}$ , 1600 rpm). Catalyst:  $\text{Pt}_{59}\text{V}_{11}\text{Fe}_{30}/\text{C}$  (45% metal loading).

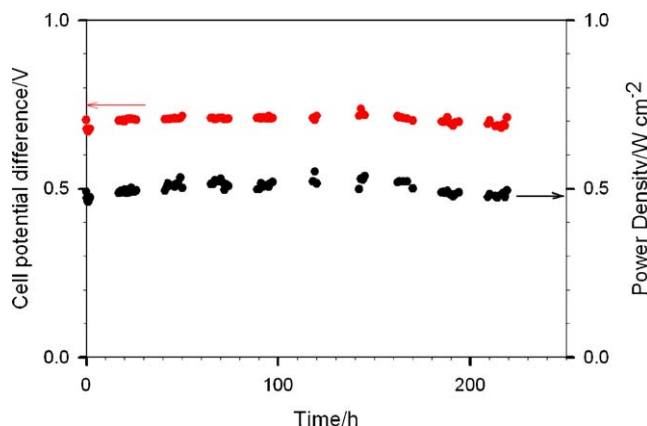


**Fig. 7.** Stability evaluation of  $\text{Pt}_{42}\text{V}_{19}\text{Fe}_{39}/\text{C}$  catalysts in PEMFC: cell potential difference and power density under  $0.7 \text{ A cm}^{-2}$  as a function of time.

The stability of the trimetallic catalysts was also examined under the fuel cell testing condition. The fuel cell testing of the same trimetallic catalysts under  $700 \text{ mA cm}^{-2}$  showed no indication of decrease in cell voltage over a week (Fig. 7). While further long-term durability test is underway, the preliminary results showed that these trimetallic catalysts, with further refinements, could lead to promising application in practical PEM fuel cells.

#### 4. Conclusions

In summary, the nano-engineered trimetallic PtVFe nanoparticle catalysts have been shown to exhibit enhanced electrocatalytic performance in PEM fuel cells. This conclusion has been substantiated by both rotating disk electrode for ORR and membrane electrode assembly measurement in PEMFC in comparison with commercial Pt/C catalysts. The electrocatalytic activities obtained from the RDE ORR and MEA FC measurements exhibited good agreement in terms of the dependence on the particle size, the

trimetallic composition, and the thermal treatment condition. The results have also demonstrated good stability of the nano-engineered trimetallic catalysts, which are potentially useful for practical applications in PEMFCs. Considering the fact that the electrocatalytic properties of bimetallic or trimetallic catalysts are affected by a combination of electronic and geometric parameters (e.g., Pt–Pt distance, d-band vacancy, particle size, and surface structure) which are dependent on catalyst-preparation and treatment methods [30], a detailed correlation of the activity and stability data with these parameters requires further systematic investigation. To improve the fuel cell performance of the nano-engineered catalysts in practical fuel cells, part of our on-going work include in-depth characterizations of these electronic and geometric parameters with a series of bimetallic and trimetallic nanoparticle catalysts prepared in our laboratory.

#### Acknowledgements

The research work was supported by the National Science Foundation (CBET-0709113).

#### References

- [1] H.A. Gasteiger, S.S. Kocha, B. Sompalli, F.T. Wagner, *Appl. Catal. B: Environ.* 56 (2005) 9.
- [2] C.J. Zhong, J. Luo, P. Njoki, D. Mott, B. Wanjala, R. Loukrakpam, S. Lim, L. Wang, B. Fang, Z. Xu, *Energy Environ. Sci.* 1 (2008) 454.
- [3] J. Luo, L. Han, N. Kariuki, L. Wang, D. Mott, C.J. Zhong, T. He, *Chem. Mater.* 17 (2005) 5282.
- [4] J. Luo, N. Kariuki, L. Han, L. Wang, C.J. Zhong, T. He, *Electrochim. Acta* 51 (2006) 4821.
- [5] X. Wang, N. Kariuki, J.T. Vaughey, J. Goodpaster, R. Kumar, D.J. Myers, *J. Electrochem. Soc.* 155 (2008) B602.
- [6] E. Ding, K.L. More, T. He, *J. Power Sources* 175 (2008) 794.
- [7] Z.D. Wei, Y.C. Feng, L. Li, M.J. Liao, Y. Fu, C.X. Sun, Z.G. Shao, P.K. Shen, *J. Power Sources* 180 (2008) 84.
- [8] K.C. Neyerlin, R. Srivastava, C. Yua, P. Strassera, *J. Power Sources* 186 (2009) 261.
- [9] J.F. Whitacre, T.J. Valdez, S.R. Narayanan, *Electrochim. Acta* 53 (2008) 3680.
- [10] J. Luo, P.N. Njoki, Y. Lin, L. Wang, D. Mott, C.J. Zhong, *Electrochem. Commun.* 8 (2006) 581.
- [11] J. Luo, L.Y. Wang, D. Mott, P.N. Njoki, Y. Lin, T. He, Z. Xu, B. Wanjala, S.I. Lim, C.J. Zhong, *Adv. Mater.* 20 (2008) 4342.
- [12] T. He, E. Kreidler, L. Xiong, J. Luo, C.J. Zhong, *J. Electrochem. Soc.* 153 (2006) A1637.
- [13] T. He, E. Kreidler, L. Xiong, E. Ding, *J. Power Sources* 165 (2007) 87.
- [14] R. Baker, D.P. Wilkinson, J. Zhang, *Electrochim. Acta* 54 (2009) 3098.
- [15] T. Inasaki, S. Kobayashi, *Electrochim. Acta* 54 (2009) 4893.
- [16] J. Li, F. Ye, L. Chen, T. Wang, J. Li, X. Wang, *J. Power Sources* 186 (2009) 320.
- [17] I. Esparb , E. Brillas, F. Centellas, J.A. Garrido, R.M. Rodr guez, C. Arias, P.-L. Cabot, *J. Power Sources* 190 (2009) 201.
- [18] S. Chen, W. Sheng, N. Yabuuchi, P.J. Ferreira, L.F. Allard, Y. Shao-Horn, *J. Phys. Chem. C* 113 (2009) 1109.
- [19] P. Yu, M. Pemberton, P. Plasse, *J. Power Sources* 144 (2005) 11.
- [20] G. Tamizhmani, G.A. Capuano, *J. Electrochem. Soc.* 141 (1994) L132.
- [21] J. Shim, D.Y. Yoo, J.S. Lee, *Electrochim. Acta* 45 (2000) 1943.
- [22] A. Seo, J. Lee, K. Han, H. Kim, *Electrochim. Acta* 52 (2006) 1603.
- [23] B. Fang, J. Luo, P.N. Njoki, R. Loukrakpam, D. Mott, B. Wanjala, X. Hu, C.J. Zhong, *Electrochem. Commun.* 11 (2009) 1139.
- [24] Z. Tang, C.K. Poh, K.K. Lee, Z. Tian, D.H.C. Chua, J. Lin, *J. Power Sources* 195 (2010) 155.
- [25] K. Su rez-Alc ntara, O. Solorza-Feria, *J. Power Sources* 192 (2009) 165.
- [26] K.J.J. Mayrhofer, D. Strmcnik, B.B. Blizanac, V. Stamenkovic, M. Arenz, N.M. Markovic, *Electrochim. Acta* 53 (2008) 3181–3188.
- [27] Electrochem, Inc., Manual SN4737, 08/04/05.
- [28] M. Prasanna, E.A. Cho, T.H. Lim, I.H. Oh, *Electrochim. Acta* 53 (2008) 5434.
- [29] M.S. Saha, A.F. Gull , R.J. Allen, S. Mukerjee, *Electrochim. Acta* 51 (2006) 4680.
- [30] C.J. Zhong, J. Luo, B. Fang, B.N. Wanjala, P.N. Njoki, R. Loukrakpam, J. Yin, *Nanotechnology* 21 (2010) 062001.